Journal of Photochemistry and Photobiology A: Chemistry 212 (2010) 113–121

Contents lists available at ScienceDirect

Journal of Photochemistry and Photobiology A: Chemistry

journal homepage: www.elsevier.com/locate/jphotochem

Photocatalytic nitrate reduction over Pt–Cu/TiO_2 catalysts with benzene as hole scavenger

Liyuan Li, Zhaoyi Xu*, Fengling Liu, Yun Shao, Jiahong Wang, Haiqin Wan, Shourong Zheng*

State Key Laboratory of Pollution Control and Resource Reuse, School of the Environment, Nanjing University, Hankou Road 22, Nanjing 210093, PR China

ARTICLE INFO

Article history:
Received 1 September 2009
Received in revised form 11 January 2010
Accepted 3 April 2010
Available online 13 April 2010

Keywords:
Nitrate
Benzene
Photocatalysis
Pt–Cu/TiO_2 catalyst

ABSTRACT

Nitrate and benzene are commonly identified contaminants in groundwater. In this study, a series of TiO_2 supported Pt–Cu bimetallic catalysts were prepared and photocatalytic nitrate reduction in the presence of benzene was investigated. The catalysts were characterized by XRD, N_2 adsorption, TEM, X-ray photoelectron spectroscopy and IR spectroscopy of CO adsorption. The results showed that Pt–Cu alloy was formed in TiO_2 supported bimetallic catalysts except for the bimetallic catalyst with TiO_2 calcined at 700 °C as the support. In addition, higher alloy dispersion and smaller metal particle sizes could be obtained on TiO_2 calcined at 300 °C compared to those calcined at 500 and 700 °C. For photocatalytic nitrate reduction in the presence of benzene, nitrate was mainly converted to ammonia or nitrite over Pt/TiO_2 or Cu/TiO_2, respectively, whereas TiO_2 supported Pt–Cu bimetallic catalysts exhibited a considerable N_2 selectivity for photocatalytic nitrate reduction. The catalytic activity and N_2 selectivity of the supported bimetallic catalyst was strongly dependent on TiO_2 calcination temperature, Pt/Cu ratio and metal loading amount. The bimetallic catalyst with TiO_2 calcined at 300 °C as the support, Pt loading amount of 5 wt.% and Pt/Cu ratio of 4/1 displayed higher N_2 selectivity compared with other bimetallic catalysts. The present results demonstrate the selective nitrate reduction over Pt–Cu/TiO_2 catalysts with benzene as the hole scavenger, highlighting the validity of simultaneous removal of aqueous nitrate and benzene by photocatalysis.

1. Introduction

Groundwater serves as an important drinking water source in the world, whereas groundwater environment is highly vulnerable to human activity-related contamination. Nitrate contamination originating from agricultural activities and urban development is ubiquitous in groundwater and may pose serious risks to human health [1]. Moreover, nitrate is usually present together with a complex suite of organic contaminants, among which petroleum hydrocarbons are frequently identified in groundwater due to accidental surface release and improper disposal of petroleum products [2]. As one of the priority pollutants regulated by the U.S. Environmental Protection Agency [3] benzene is unanimously considered to be the most recalcitrant toward biotic degradation among petroleum hydrocarbons [4,5]. To comply with corresponding regulations, a variety of treatment methods have been developed to effectively remove nitrate or benzene in groundwater [6–9].

It has been well recognized that photocatalysis is capable of eliminating inorganic or organic pollutants in water via either oxidation or reduction mechanism. The photocatalytic pollutant abatement is implemented via the excitation of electrons from the valence band to the conduction band of the semiconductor upon absorption of photons with energy greater or equal to the band gap energy, by which the excited electrons or holes can be further utilized to reduce or oxidize pollutants [10–12].

Benzene in water can be degraded and eventually mineralized using the photocatalytic approach. For example, Izumi et al. [13] studied the photocatalytic benzene degradation over TiO_2 and platinized TiO_2 in water and detected intermediate phenol and mineralization product CO_2. Turchi and Ollis [9] systematically studied photocatalytic decomposition of benzene in TiO_2 slurry system and found that the benzene decomposition processed via the hydroxylation of benzene to generate primary degradation intermediates, such as phenol and quinone, followed by complete mineralization. Furthermore, Hashimoto et al. [14] investigated the photocatalytic degradation of aliphatic and aromatic compounds and observed considerable H_2 evolution during benzene degradation over Pt/TiO_2.

Photocatalytic nitrate reduction has also been intensively investigated. It is general consensus that the presence of hole scavenger is essential for the effective nitrate reduction although direct nitrate reduction has been also attempted in the absence of hole scavenger [15–17]. In addition, hole scavenger type plays a crucial role in the photocatalytic nitrate reduction. Different hole scavengers, such as

* Corresponding authors. Tel.: +86 25 83595831; fax: +86 25 83707304.
E-mail addresses: zhaoyixu@nju.edu.cn (Z. Xu), srzheng@nju.edu.cn (S. Zheng).

1010-6030/$ – see front matter © 2010 Elsevier B.V. All rights reserved.
doi:10.1016/j.jphotochem.2010.04.003

alcohols, small molecule organic acids and humic acid, were tested in the photocatalytic nitrate reduction and formic acid was proven to be the most effective one in terms of nitrate conversion and N_2 selectivity [18–22]. Moreover, nitrate reduction is strongly dependent on the properties of the photocatalysts. For example, Ohtani et al. [23] studied the photocatalytic reduction of nitrate over TiO_2 and attributed the low photocatalytic activity of TiO_2 to the low tendency of nitrate to react directly with excited electrons. Kominami et al. [24] compared different metallized TiO_2 catalysts for nitrate reduction and found that Ag or Cu loaded TiO_2 showed the highest activity and NH_3 selectivity. Gao et al. [25] studied photocatalytic nitrate reduction over TiO_2 supported monometallic and bimetallic catalysts in the presence of oxalic acid and concluded that Ni–Cu/TiO_2 was effective for the selective nitrate reduction. Kominami et al. [21] first observed the selective reduction of aqueous nitrate to N_2 over TiO_2 supported Pd and Pd–Cu catalysts in the presence of oxalate anions. Zhang et al. [22] studied nitrate reduction over Ag/TiO_2 with fine silver clusters and also observed selective nitrate reduction to nitrogen with substantially higher nitrate reduction efficiency than that of catalytic nitrate hydrogenation. More recently, Sá et al. [18] systematically investigated the photocatalytic nitrate reduction on metal modified TiO_2 catalysts and highly effective nitrate reduction were achieved over silver modified titania Hombikat with formic acid as the hole scavenger. It should be emphasized that in the literatures small molecule organic acids were artificially introduced as the effective hole scavengers for photocatalytic nitrate reduction. Nitrate reduction by photocatalytic approach with organic pollutants as hole scavengers has not yet, to our knowledge, been reported.

The goal of this work was to study the photocatalytic nitrate reduction over metallized TiO_2 catalysts with benzene as the hole scavenger considering the common occurrence of nitrate and benzene in groundwater. A series of TiO_2 supported monometallic and bimetallic catalysts were prepared and characterized by XRD, N_2 adsorption, TEM, XPS and IR spectroscopy of CO adsorption. The impacts of catalyst properties on the photocatalytic nitrate reduction were systematically investigated.

2. Experimental

2.1. Catalyst preparation

TiO_2 precursor was prepared using the sol–gel method. Briefly, a mixture of 20 ml distilled water and 20 ml isopropanol was added slowly to a mixture of 40 ml titanium tetraisobutyloxide and 200 ml isopropanol under vigorous stirring. The resulting gel was recovered by centrifugation followed by repeated washing with distilled water. TiO_2 precursor was subsequently obtained by drying the gel at 80 °C for 12 h. Different TiO_2 supports were prepared by calcining TiO_2 precursor at 300, 500 and 700 °C for 4 h. TiO_2 support calcined at 300, 500 or 700 °C is referred to as Ti300, Ti500 or Ti700, respectively.

Supported monometallic and bimetallic catalysts were prepared using the conventional wet impregnation method. Typically, TiO_2 support was impregnated by H_2PtCl_6 or/and $Cu(NO_3)_2$ solution followed by drying at 100 °C for 2 h, calcining at 300 °C under air for 2 h and subsequently reducing at 300 °C under H_2 atmosphere for 4 h. The resulting monometallic or bimetallic catalyst is denoted as Pt(x)–Cu(y)/Tiz, where x, y and z are Pt content (wt.%), Cu content (wt.%) and calcination temperature of TiO_2 support, respectively.

2.2. Catalyst characterization

X-ray diffraction (XRD) patterns of the catalysts were recorded on a Rigaku D/max-RA powder diffraction-meter. The average particle sizes of the samples were calculated from XRD patterns using the Scherrer equation [26]. Brunauer–Emmett–Teller (BET) surface areas of the catalysts were measured using the nitrogen adsorption method on a Micromeritics ASAP 2200 instrument at −196 °C (77 K). Transmission electron microscopy (TEM) images of the samples were collected on a Hitachi H-800 transmission electron microscope. X-ray photoelectron spectroscopy (XPS) was performed on a Perkin-Elmer PHI-550 instrument equipped with a monochromatized Al *Ka* X-ray source ($h\nu$ = 1486.6 eV) and a hemispherical electron analyzer. The C 1s peak (284.6 eV) was used for the calibration of binding energy values. The pressure in the analytical chamber was about 2×10^{-9} Pa.

CO adsorption was followed by IR spectroscopy in a vacuum IR system. The sample (approximately 10 mg) was pressed into self-supporting wafer and placed in an IR cell connected to a vacuum system. The sample was *in situ* reduced in H_2 atmosphere by heating to 300 °C at the rate of 10 °C min^{-1} and holding at this temperature for 1 h. After cooled to room temperature, the sample was exposed to 15 mbar CO for 30 min. Upon evacuation at about 10^{-5} mbar for 30 min, IR spectra were then recorded at ambient temperature using a Nicolet 5700 FT-IR spectrometer at 4 cm^{-1} resolution.

2.3. Photocatalytic reaction

Photocatalytic reaction was carried out in a NDC photo-reactor equipped with a 500 ml cylindrical Pyrex vessel irradiated directly by a high pressure mercury lamp (250 W), which is shown in Fig. S1. Preliminary experiments showed that the activity and selectivity of photocatalytic nitrate reduction over supported bimetallic catalysts in the presence of benzene was approximately identical in a pH range of 4.2–6.0. Thus all photocatalytic reactions were preformed at pH around 5.8. In a typical run, 0.5 g of the catalyst was suspended in 500 ml distilled water and the suspension system was purged by N_2 for 30 min. Nitrate solution or/and benzene stock solution was added to the suspension solution to obtain about 60 mg l^{-1} nitrate or/and 10 mg l^{-1} benzene. The suspension was further stirred in the dark for 60 min to reach the adsorption equilibrium prior to the photocatalytic test. During the photocatalytic reaction, samples were taken at selected intervals and the catalyst particles were removed by centrifugation. The residual nitrate concentration was determined using UV/Vis spectrophotometer at wavelength of 220 nm. The nitrite concentration was determined using UV/Vis spectrophotometer at 540 nm using the naphthylamine analytical procedure. The concentration of ammonium ion was analyzed using the Nessler method [27]. The residual benzene concentration in the solution was analyzed using gas chromatography equipped with a FID detector by extracting the aqueous phase with hexane and toluene was used as the internal standard. Benzene degradation intermediates, phenol, were determined using HPLC (Agilent 1200), equipped with an ultraviolet (UV) detector and a C18 reversed phase column (250 mm × 4.5 mm, 5 μm, Agilent, USA) at 30 °C. The mobile phase is acetonitrile–water (50/50, v/v) with a flow rate of 1.0 ml min^{-1}. The average activity is defined as the specific removal rate of nitrate within 4 h reaction time and N_2 selectivity is calculated according to Eq. (1):

$$S_{N_2} = \frac{[\text{nitrate}]_0 - [\text{nitrate}]_t - [\text{nitrite}]_t - [\text{ammonia}]_t}{[\text{nitrate}]_0 - [\text{nitrate}]_t} \times 100\% \quad (1)$$

where S_{N_2} is N_2 selectivity, $[\text{nitrate}]_0$ is the initial nitrate concentration, and $[\text{nitrate}]_t$, $[\text{nitrite}]_t$ and $[\text{ammonia}]_t$ are the residual concentration of nitrate, nitrite and ammonia after reaction for 4 h, respectively.

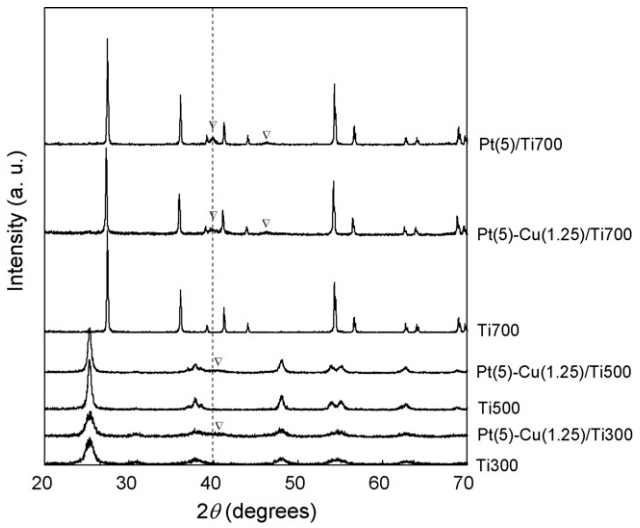

Fig. 1. XRD patterns of TiO_2 and TiO_2 supported catalysts.

3. Results and discussion

3.1. Material characterization

XRD patterns of TiO_2 samples and supported bimetallic catalysts are compared in Fig. 1. Both Ti300 and Ti500 consisted of typical anatase phase, while for Ti300 low peak intensity and broad diffraction peaks were observed, suggesting a lower content of anatase phase in Ti300 and smaller particle sizes of Ti300 compared to Ti500. Further increasing the calcination temperature of TiO_2 precursor from 500 to 700 °C led to the transformation of TiO_2 crystalline phase from anatase to rutile. The particle sizes of TiO_2 supports were calculated based on XRD patterns using Scherrer equation [26] and the results are listed in Table 1. The average particle sizes of Ti300, Ti500 and Ti700 were estimated to be 9.2, 17.0 and 63.2 nm, respectively, indicative of the increased TiO_2 particle size with increasing calcination temperature. In parallel, N_2 adsorption results showed that increasing TiO_2 calcination temperature led to decreased BET surface area of TiO_2 support due to the crystal growth at high calcination temperature [28,29]. For TiO_2 supported bimetallic catalysts, the crystalline phases and particle sizes of TiO_2 supports kept approximately identical to those before impregnation and reduction, reflecting that TiO_2 supports are virtually stable during impregnation and reduction processes. It is noteworthy that in comparison with TiO_2 supports new diffraction peaks were observed in TiO_2 supported bimetallic catalysts. In order to clearly elucidate the superficial metal properties, Pt(5)/Ti700 was prepared and its XRD pattern is also compiled in Fig. 1. For Pt(5)/Ti700, new diffraction peaks were observed with 2θ at 39.8° and 46.3°, characteristic of typical Pt metal with fcc crystallographic structure [30]. Similarly, the diffraction peaks with 2θ at 39.7° and 46.2° were also visible in Pt(5)–Cu(1.25)/Ti700, indicative of the presence of Pt metal in Pt(5)–Cu(1.25)/Ti700. For Pt(5)–Cu(1.25)/Ti300 and Pt(5)–Cu(1.25)/Ti500, however, much weaker and broader diffraction peaks were observed at about 40.9°, suggesting different metal compositions from that in Pt(5)–Cu(1.25)/Ti700. The deviation of the diffraction peak positions from those of typical Pt metal can be attributed to the formation of Pt–Cu alloy in both Pt(5)–Cu(1.25)/Ti300 and Pt(5)–Cu(1.25)/Ti500 [30], and the shift of Pt–Cu alloy diffraction peaks to large 2θ is intrinsically indicative of decreased cell parameters as a result of incorporation of Cu with comparatively small atomic radius into Pt metal lattice. Furthermore, the low peak intensities and broad diffraction peaks of Pt–Cu alloys in Pt(5)–Cu(1.25)/Ti300 and Pt(5)–Cu(1.25)/Ti500 are characteristic of metal species with relatively small particle sizes, reflecting much higher metal dispersions over Ti300 and Ti500 compared to Ti700. It should be pointed out that the similar metal diffraction peaks in Pt(5)–Cu(1.25)/Ti700 to those in Pt(5)/Ti700 suggests the absence of Pt–Cu alloy in Pt(5)–Cu(1.25)/Ti700. In principle, the formation of Pt–Cu alloy on support surface can be well interpreted using a "catalyzed reduction" mechanism [31,32]. During H_2 reduction process, metallic Pt particles are formed prior to the reduction of the Cu precursor due to the lower reduction temperature of the Pt precursor compared to the Cu precursor. The resultant Pt particles subsequently act as the catalytically active sites to provide split-over hydrogen for the reduction of surface Cu precursor, leading to the deposition of metallic Cu on Pt particle surface and to the subsequent formation of Pt–Cu alloy as a result of metallic Cu diffusion into Pt metal lattice. For Ti300 and Ti500, the high BET surface areas of TiO_2 supports lead to the facile formation of fine Pt particles, facilitating metallic Cu diffusion into Pt metal lattice and the subsequent formation of Pt–Cu alloys. In the case of Ti700, in contrast, the low specific surface of TiO_2 support results in a low Pt metal dispersion as well as large Pt particle sizes and, therefore, metallic Cu diffusion into Pt metal lattice and the formation of Pt–Cu alloy is markedly suppressed, resulting in the absence of Pt–Cu alloy in Pt(5)–Cu(1.25)/Ti700.

The findings are further supported by TEM observations of the catalysts. TEM images and histograms of metal particle size distributions of Pt(5)–Cu(1.25)/Ti300, Pt(5)–Cu(1.25)/Ti500 and Pt(5)–Cu(1.25)/Ti700 are compared in Figs. 2 and 3, respectively. For TiO_2 supported bimetallic catalysts, the particle sizes of TiO_2 supports were found to be approximately 8–14, 15–25 and 80–200 nm in Pt(5)–Cu(1.25)/Ti300, Pt(5)–Cu(1.25)/Ti500 and Pt(5)–Cu(1.25)/Ti700, respectively. Moreover, relatively small metal particles were distinguished in Pt(5)–Cu(1.25)/Ti300 and Pt(5)–Cu(1.25)/Ti500, whereas considerably large metal particles with particle sizes varied from 1 to 30 nm were identified in Pt(5)–Cu(1.25)/Ti700. As shown in Fig. 3, in parallel, much narrow distributions of metal particle sizes were observed in Pt(5)–Cu(1.25)/Ti300 and Pt(5)–Cu(1.25)/Ti500 compared with Pt(5)–Cu(1.25)/Ti700. The average metal particle sizes in Pt(5)–Cu(1.25)/Ti300, Pt(5)–Cu(1.25)/Ti500 and Pt(5)–Cu(1.25)/Ti700 were estimated to be 2.3, 3.4 and 11.7 nm, respectively, indicating much smaller metal particle sizes in Pt(5)–Cu(1.25)/Ti300 and Pt(5)–Cu(1.25)/Ti500 compared to

Table 1
Structural properties of TiO_2 and TiO_2 supported bimetallic catalysts.

Sample	TiO_2 crystalline phase	S_{BET} ($m^2\ g^{-1}$)	TiO_2 particle size (nm)		Average metal particle size (nm)
			XRD	TEM	
Ti300	Anatase	131.5	9.2	–	–
Pt(5)–Cu(1.25)/Ti300	Anatase	105.9	8.9	8–14	2.3
Ti500	Anatase	59.9	17.0	–	–
Pt(5)–Cu(1.25)/Ti500	Anatase	56.9	17.4	15–25	3.4
Ti700	Rutile	1.1	63.2	–	–
Pt(5)–Cu(1.25)/Ti700	Rutile	1.0	63.2	80–200	11.7

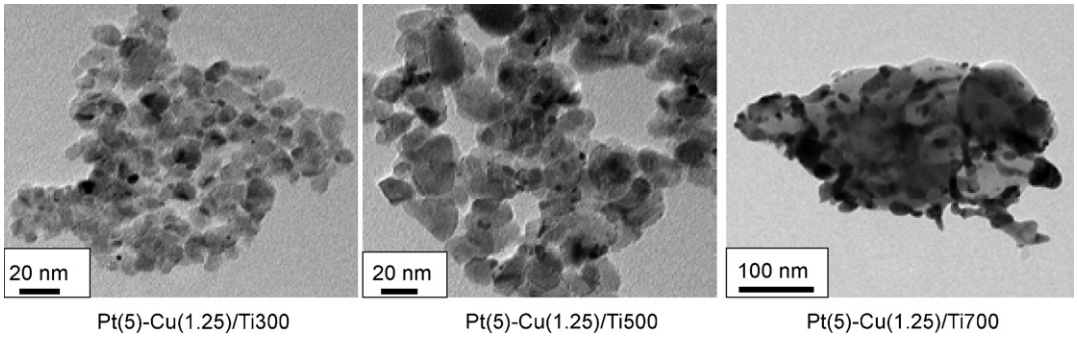

Fig. 2. Transmission electron micrographs of Pt(5)–Cu(1.25)/Ti300, Pt(5)–Cu(1.25)/Ti500 and Pt(5)–Cu(1.25)/Ti700.

Pt(5)–Cu(1.25)/Ti700. This further demonstrates that metallic species can be well dispersed over TiO_2 support calcined at low temperature.

XPS analysis can provide information of the oxidation states and compositions of the superficial metals. The XPS spectra of Pt(5)–Cu(1.25)/Ti300, Pt(5)–Cu(1.25)/Ti500 and Pt(5)–Cu(1.25)/Ti700 in the Cu 2p and Pt 4f regions are depicted in Fig. 4. The Cu 2p and Pt 4f spectra normalized by the corresponding atomic sensitivity factors were used to determine surface atomic concentrations [33]. Pt surface concentrations were calculated using the Pt 4f spectra by subtracting Cu 3p peak estimated from the Cu 2p spectra because Pt 4f spectra were partially overlapped by the Cu 3p spectra. The parameters of XPS spectra and estimated surface metal ratios are listed in Table 2. As shown in Fig. 4a, the binding energies of the Cu core line $2p_{3/2}$ were centered at about 932.3 eV, reflecting the presence of Cu^0 in the supported bimetallic catalysts [34]. It is noteworthy that in Pt(5)–Cu(1.25)/Ti700 a well resolved shake-up satellite was observed at 943.6 eV, characteristic of the multiple splitting from typical Cu^{2+} species [35]. Larsson and Andersson [35] concluded that the intensity ratio of the Cu 2p shake-up satellite to the Cu $2p_{3/2}$ peak varied from 0.42 to 0.52 for CuO/TiO_2 catalysts. However, the ratio of the shake-up satellite to the Cu $2p_{3/2}$ peak in Pt(5)–Cu(1.25)/Ti700 was found to be 0.24 and the lower ratio suggests the presence of both Cu^0 and Cu^{2+} species, probably due to the partial oxidation of metal Cu upon exposure to air. In contrast, the shake-up satellite characteristic of Cu^{2+} species was absent in both Pt(5)–Cu(1.25)/Ti300 and Pt(5)–Cu(1.25)/Ti500, which can be attributed to the stabilization of metal Cu against oxidation via formation of Pt–Cu alloy [36]. For the Pt 4f spectra, the Pt 4f signal consisted of typical doublet with Pt $f_{7/2}$ located at around 71.4 eV, assigned to metallic Pt [37,38]. The Pt/Cu atomic ratios were estimated to be 1.02, 1.04 and 0.23 for Pt(5)–Cu(1.25)/Ti300, Pt(5)–Cu(1.25)/Ti500 and Pt(5)–Cu(1.25)/Ti700, respectively, indicative of considerable surface Cu enrichment in the catalysts probably associated with the aggregation of metallic Cu over Pt surface. It should be pointed out that Pt/Cu ratio in Pt(5)–Cu(1.25)/Ti300 is approximately identical to that in Pt(5)–Cu(1.25)/Ti500 and markedly higher than that in Pt(5)–Cu(1.25)/Ti700, which mainly results from the facile diffusion of metallic Cu into Pt lattice and the formation of Pt–Cu alloy in Pt(5)–Cu(1.25)/Ti300 and Pt(5)–Cu(1.25)/Ti500.

Table 2
Parameters of XPS spectra and surface atom ratios.

Sample	Binding energy (eV)		Atomic ratio
	Pt $4f_{7/2}$	Cu $2p_{3/2}$	Pt/Cu
Pt(5)–Cu(1.25)/Ti300	71.4	932.2	1.02
Pt(5)–Cu(1.25)/Ti500	71.4	932.1	1.04
Pt(5)–Cu(1.25)/Ti700	71.6	932.4	0.23

Fig. 5a shows IR spectra of CO adsorption on different catalysts after evacuation at room temperature for 30 min. For Pt(5)/Ti300, a broad IR band around 2080 cm^{-1} with a shoulder at 2052 cm^{-1} and a weak IR band around 1846 cm^{-1} were observed. The broad IR band with maximum at 2080 cm^{-1} and a shoulder at 2052 cm^{-1} are assigned to linear CO adsorption [39–41] and the broad nature of linear CO adsorption can be attributed to either CO adsorption on the planes, edges and corners of Pt particles or CO adsorption on Pt crystallites with varied particle sizes [42]. The weak IR band around 1846 cm^{-1} is assigned to the bridged form of adsorbed CO on Pt particles [43,44]. For CO adsorption on Pt(5)–Cu(1.25)/Ti300 and Pt(5)–Cu(1.25)/Ti500, similar IR patterns were obtained and the IR bands characteristic of linear CO adsorption were observed at 2048 cm^{-1}, indicative of a considerable red shift of linear CO adsorption compared with that on Pt(5)/T300. Shpiro et al. [45] studied HZSM-5 supported Pt–Cu alloy and attributed the red shift of IR bands characteristic of linear CO adsorption to the electron donation of Cu to Pt. In addition, the similar IR band position of linear CO adsorption over Pt(5)–Cu(1.25)/Ti300 to that over Pt(5)–Cu(1.25)/Ti500 implies similar surface compositions of Pt–Cu alloys, which is consistent with the similar Pt/Cu ratios of the catalysts (see Table 2). For Pt(5)–Cu(1.25)/Ti700, however, the bands characteristic of CO adsorption on Pt were not observed. This can be ascribed to the low adsorbed CO concentration resulting from both Cu enrichments over Pt surface as indicated by XPS analysis and large Pt particles [41]. The surface properties of Pt–Cu alloy are also correlated to Pt/Cu ratio in the bimetallic catalyst. IR spectra of CO adsorption on the supported bimetallic catalysts with varied Pt/Cu ratios are compiled in Fig. 5b. IR bands characteristic of linear CO adsorption were observed at 2080, 2058, 2048 and 2035 cm^{-1} for Pt(5)/T300, Pt(5)–Cu(0.83)/Ti300, Pt(5)–Cu(1.25)/Ti300 and Pt(5)–Cu(2.5)/Ti300, respectively, indicative of an increased red shift as well as increased Cu content in Pt–Cu alloy with the increase of Cu content in the bimetallic catalysts.

3.2. Photocatalytic nitrate reduction

3.2.1. Photocatalytic mechanism

For photocatalytic nitrate reduction over Ti300, Cu/Ti300, Pt/Ti300 or Pt–Cu/Ti300, no distinct nitrate conversion was observed after photocatalytic reaction for 4 h probably due to the absence of the hole scavenger in the reaction systems. In the presence of 10 mg l^{-1} benzene, photocatalytic nitrate reduction over Ti300, Cu(1.25)/Ti300 and Pt(5)/Ti300 is described in Fig. 6. For Ti300, minor nitrate was found to be converted to ammonia. Ohtani et al. [23] studied photocatalytic nitrate reduction on TiO_2 with 2-propanol as the hole scavenger and observed low nitrate conversion, which was attributed to the incapability of directly utilizing the excited electrons by nitrate. In contrast, Sá et al. [18] observed substantial nitrate conversion over TiO_2 with formic acid as the hole scavenger, suggesting that photocatalytic nitrate reduction over

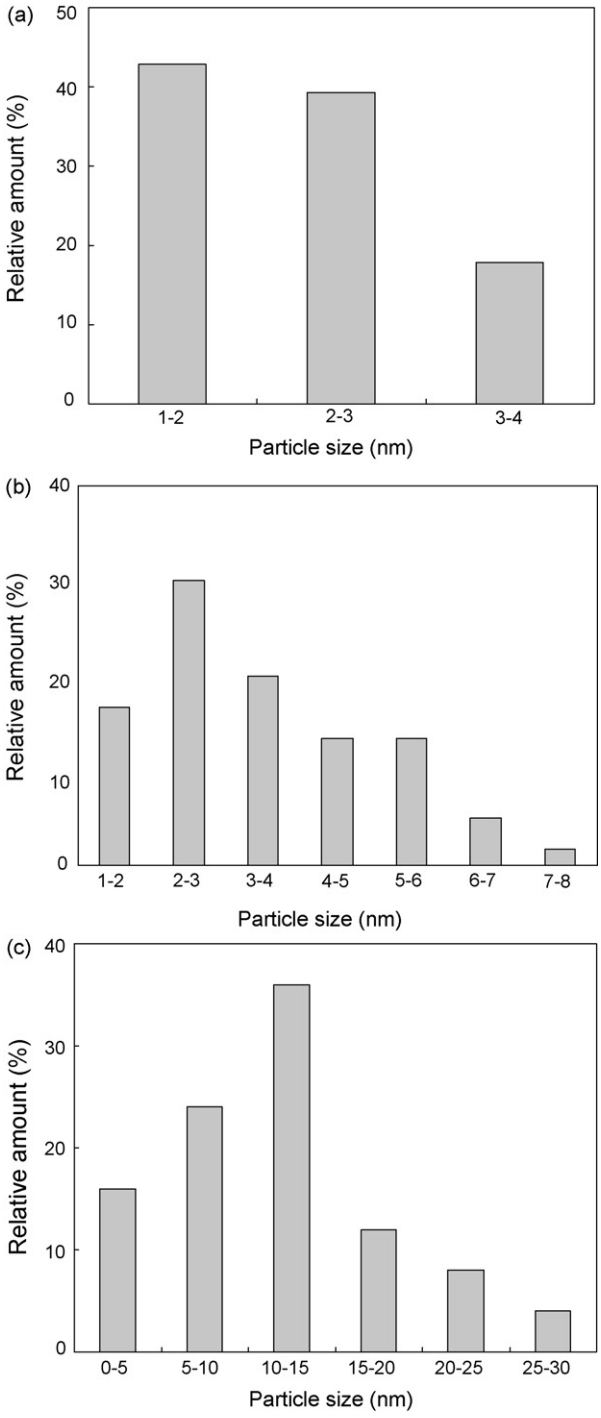

Fig. 3. Histograms of metal particle size distribution in (a) Pt(5)–Cu(1.25)/Ti300, (b) Pt(5)–Cu(1.25)/Ti500 and (c) Pt(5)–Cu(1.25)/Ti700.

TiO_2 is highly dependent on the nature of hole scavenger. For photocatalytic nitrate reduction with formic acid as the hole scavenger, Sá et al. and Zhang et al. suggested that nitrate could be effectively reduced by reductive carboxyl anion radicals generated from photocatalytic formic acid decomposition [18,22,46]. However, Teoh et al. [47] pointed out that unlike formic acid no reductive radicals were directly generated during photocatalytic phenol degradation. In parallel, the absence of reductive radicals from photocatalytic benzene degradation can be reasonably expected due to its similar degradation pathway to that of phenol. It should be pointed out that prior to the complete mineralization of benzene a variety of

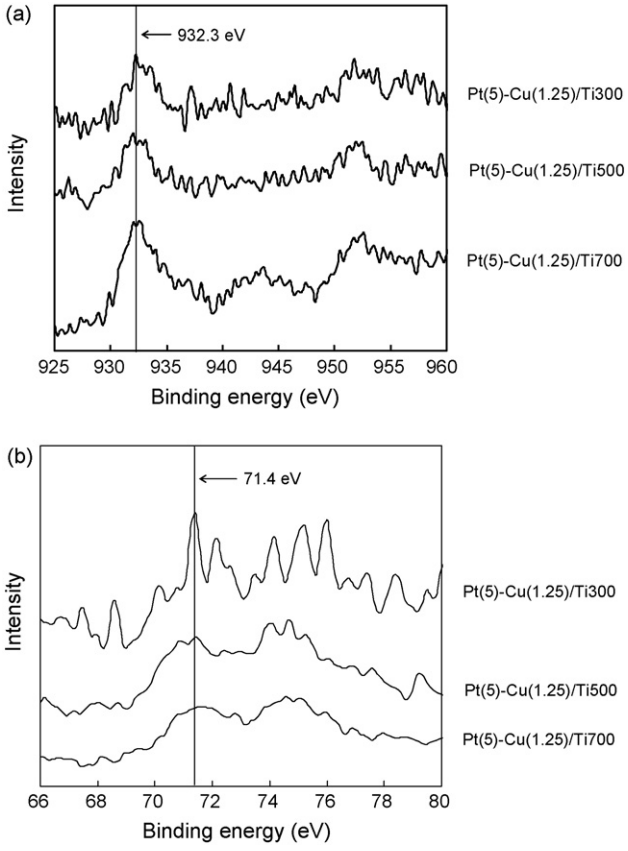

Fig. 4. XPS spectra of (a) the Cu 2p region and (b) the Pt 4f region.

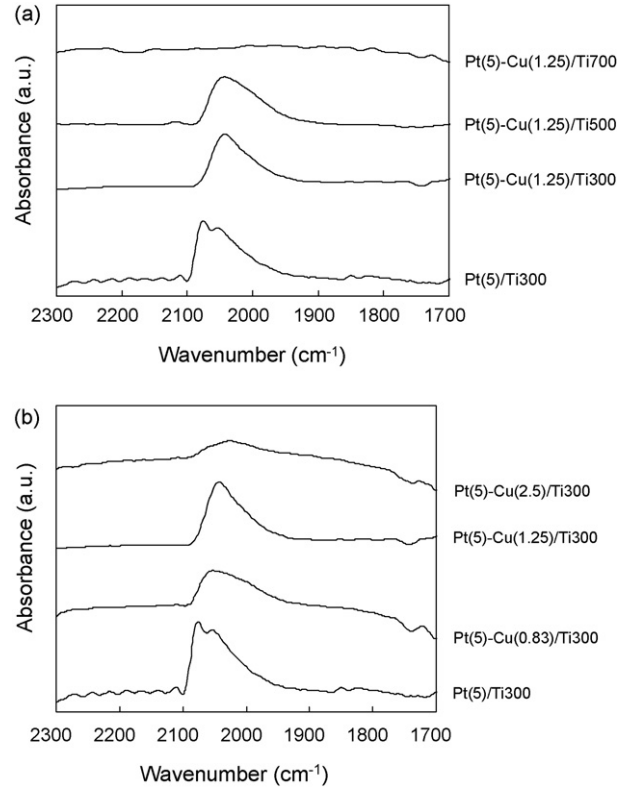

Fig. 5. CO adsorption IR of TiO_2 supported monometallic and bimetallic catalysts.

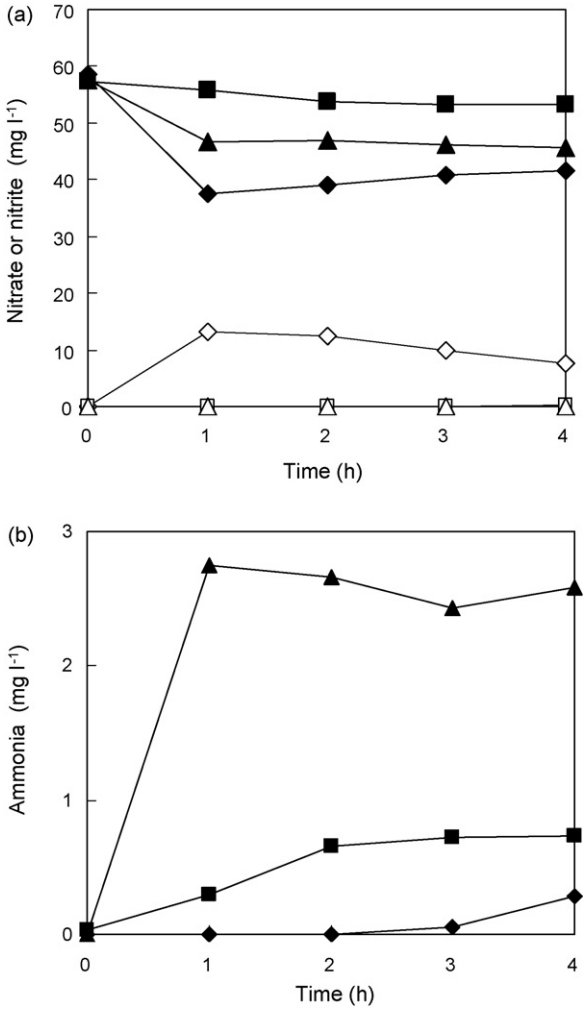

Fig. 6. (a) Nitrate reduction over (■, □) Ti300, (▲, △) Pt(5)/Ti300 and (♦, ◊) Cu(1.25)/Ti300. Filled symbols denote nitrate concentration and open symbols denote nitrite concentration. (b) Concentration profiles of ammonia as a function of reaction time over (■) Ti300, (▲) Pt(5)/Ti300 and (♦) Cu(1.25)/Ti300.

small molecule organic acids can be formed [9,13,14]. These small molecule organic acids may serve as the precursors of reductive radicals for nitrate reduction, reflected by the fact that photocatalytic nitrate reduction over Ti300 mainly occurs in the later reaction stage instead of the initial stage. It should be emphasized that due to the relatively low concentration of small molecule organic acids generated during photocatalytic benzene degradation nitrate reduction directly by reductive radicals only plays a minor role, evidenced by the fact that only minor nitrate was converted with TiO_2 as the photocatalyst.

For Cu(1.25)/Ti300, a substantial amount of nitrate was converted to nitrite after reaction for 1 h and the nitrite concentration gradually decreased in concomitance with the slow increase of nitrate concentration in succedent 3 h. Bae et al. [48] studied nitrate adsorption on Cu(1 0 0) and observed the reduction of nitrate to nitrite. Epron et al. [49] further pointed out that nitrate could be feasibly reduced by metallic Cu via a chemical redox mechanism. Therefore, the evolution of nitrite during photocatalytic nitrate reduction over Cu(1.25)/Ti300 is understandable assuming the directly reduction of nitrate by metallic Cu to nitrite via a chemical redox process. It is noteworthy that after photocatalytic reaction for 1 h approximately 37% nitrate is converted to nitrite, which is stoichiometrically higher than the Cu content in Cu(1.25)/Ti300. This suggests a photocatalytic process involved in

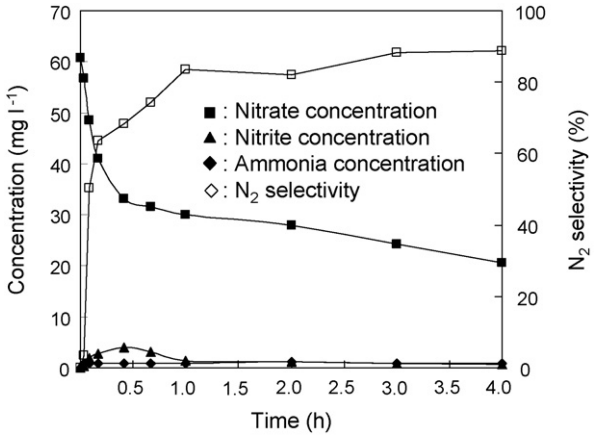

Fig. 7. Photocatalytic nitrate reduction over Pt(5)–Cu(1.25)/Ti300.

the nitrate reduction over Cu(1.25)/Ti300, by which the oxidized Cu is photocatalytically reduced by excited electrons in the presence of hole scavenger. After the depletion of hole scavenger, nitrite oxidation to nitrate over TiO_2 surface dominates [50], leading to the continuous conversion of nitrite to nitrate. As for photocatalytic nitrate reduction over Pt(5)/Ti300, approximately 20% nitrate was selectively converted to ammonia in the initial reaction stage. Kudo et al. observed enhanced nitrate conversion to ammonia after platinization of TiO_2 and $SrTiO_3$ and attributed the enhanced conversion to nitrate reduction by H_2 on Pt surface [51,52]. It should be pointed out that H_2 evolution is usually observed during the photocatalytic decomposition of organic pollutants over platinized TiO_2 [14,53]. It is noteworthy that after photocatalytic reaction for 4 h the sum of nitrate, nitrite and ammonia were found to be 0.91, 0.90 and 0.88 mmol l^{-1} for nitrate reduction over Ti300, Cu(1.25)/Ti300 and Pt(5)/Ti300, respectively, approximately identical to that of initial nitrate concentration (0.92 mmol l^{-1}), implying that there is not direct reaction between nitrate, nitrite or ammonia and organic species under our reaction conditions, and no N_2 selectivity can be achieved in the presence of TiO_2 or supported monometallic catalyst.

In contrast to supported monometallic catalysts, TiO_2 supported bimetallic catalysts exhibited very different catalytic behavior for photocatalytic nitrate reduction. The photocatalytic removal of nitrate over Pt(5)–Cu(1.25)/Ti300 is compiled in Fig. 7. Nitrate concentration prominently decreased in first 20 min and slowly declined afterwards. In addition, the intermediates and products from nitrate reduction, nitrite and ammonia, were also identified. The evolution of nitrite was found to be in the first 60 min with a maximum concentration of 4.0 mg l^{-1} at 25 min and the majority of ammonia was formed in the first 20 min and remained approximately identical afterwards. The observed decreased catalytic activity of Pt(5)–Cu(1.25)/Ti300 after reaction for 20 min is probably due to catalyst deactivation or depletion of hole scavenger during the reaction process. To verify catalyst stability, the catalyst was recycled and the catalytic activities of the first and second recycled catalyst were found to be 59% and 37% of the fresh catalyst after photocatalytic nitrate reduction for 4 h (see Fig. S2), indicative of gradual deactivation of the catalyst for photocatalytic nitrate reduction. To verify possible Cu leaching from the catalyst, the solution after photocatalytic reaction was subjected to atomic absorption spectroscopy analysis (Hitach Z-8100, Japan) and no Cu^{2+} was detected in the solution, implying that the catalyst deactivation possibly results from irreversible adsorption of degradation products.

In parallel, benzene degradation was also monitored and the result is presented in Fig. S3. Benzene as well as its degra-

dation product phenol was completely degraded within first 10 min, suggesting that the markedly declined catalytic activity of Pt(5)–Cu(1.25)/Ti300 may also related to the depletion of hole scavenger. Considering benzene depletion during nitrate reduction, the influence of benzene concentration on photocatalytic nitrate reduction was investigated and the result is shown in Fig. S4. Increasing benzene concentration from 5 to 10 mg l^{-1} led to the increased activity from 7.3 to 9.1 mg h^{-1} $g_{cat}{}^{-1}$, whereas further increase of benzene concentration resulted in decreased catalytic activity, probably due to the inhibited nitrate adsorption over the catalyst by increased benzene concentration. It is interesting to note that after benzene and its primary degradation products, e.g. phenol, are completely degraded nitrate concentration slowly decreases, suggesting that other intermediates from benzene degradation, such as small molecule organic acids, can also serve as effective hole scavengers.

As shown in Fig. 7 Pt(5)–Cu(1.25)/Ti300 displayed considerable N_2 selectivity, indicating that the coexistence of metallic Cu and Pt is crucial for selective nitrate reduction. For Pt(5)–Cu(1.25)/Ti300, the results of XRD, CO adsorption IR and XPS analysis demonstrate the presence of Pt–Cu alloy on Ti300 surface. Therefore, nitrate can be feasibly reduced to nitrite by metallic Cu via a redox process. The oxidized Cu can be subsequently reduced either directly by excited electrons or mediated by Pt [54,55], which reactivates the bimetallic catalyst and facilitates the further reduction of nitrate to nitrite. The resultant nitrite tends to be chemically adsorbed on metallic Pt sites due to its strong adsorption affinity to metallic Pt sites [56], leading to the consequent reduction of nitrite to N_2 or ammonia by H_2 on Pt surface.

Based on above analysis, the possible mechanism for photocatalytic nitrate reduction with benzene as the hole scavenger over TiO_2 supported Pt–Cu bimetallic catalyst can be briefly summarized as follows:

$$Pt\text{–}Cu/TiO_2 + h\nu \rightarrow e_{CB}{}^- + h_{VB}{}^+ \quad (2)$$

$$NO_3{}^- + Cu \rightarrow Cu^{\delta+} + NO_2{}^- \quad (3)$$

$$Benzene + h_{VB}{}^+ \rightarrow intermediates + h_{VB}{}^+ \rightarrow CO_2 \quad (4)$$

$$H^+ + e_{CB}{}^-/Pt \rightarrow (1/2)H_2/Pt \quad (5)$$

$$Cu^{\delta+} + e_{CB}{}^-/Pt \rightarrow Cu \quad (6)$$

$$2NO_2{}^- + 2H^+ + 3H_2/Pt \rightarrow N_2 + 4H_2O \quad (7)$$

$$NO_2{}^- + H^+ + (6/2)H_2/Pt \rightarrow NH_3 + 2H_2O \quad (8)$$

$$NO_2{}^- + H_2O^+ + 2h_{VB}{}^+ \rightarrow NO_3{}^- + 2H^+ \quad (9)$$

3.2.2. Influence of catalyst properties on the removal of benzene and nitrate

The supported bimetallic catalyst structurally consists of TiO_2 support and superficial metals. TiO_2 support is responsible for the generation of charge carriers upon light irradiation and for subsequent benzene degradation. Superficial metals act as the appropriate active sites for the reduction of nitrate and nitrite. The delicate interplay between TiO_2 support and superficial metals may play an important role in controlling the activity and selectivity of the bimetallic catalyst for the photocatalytic nitrate reduction. For example, superficial metal dispersion and alloy composition is closely linked to TiO_2 properties, while surface metallization of TiO_2 may exert marked impact on TiO_2 photo-induction efficiency via formation of Schottky-type barrier, blocking of oxidation sites [57,58], and shield-effect [59,60].

TiO_2 property is dependent on calcination temperature, which may directly influence the catalytic activity and selectivity of the supported bimetallic catalyst. For supported bimetallic catalysts, benzene as well as the primary intermediates was found

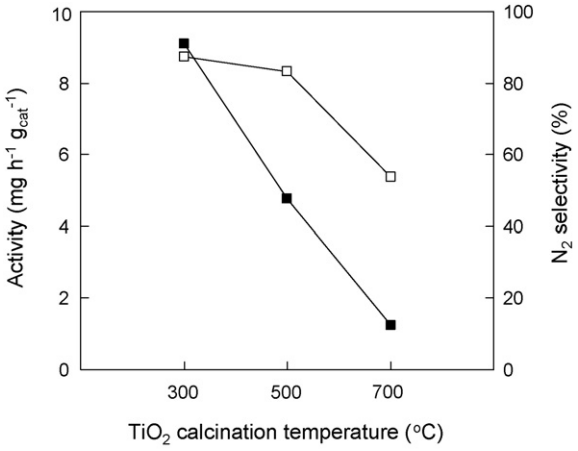

Fig. 8. Catalytic activities and N_2 selectivities of Pt(5)–Cu(1.25)/Ti300, Pt(5)–Cu(1.25)/Ti500 and Pt(5)–Cu(1.25)/Ti700. Filled symbols denote catalytic activities and open symbols denote N_2 selectivities.

to be fast degraded within 10 min and, therefore, only nitrate reduction will be discussed in details afterward. After reaction for 4 h, the activities and N_2 selectivities of Pt(5)–Cu(1.25)/Ti300, Pt(5)–Cu(1.25)/Ti500 and Pt(5)–Cu(1.25)/Ti700 are compiled in Fig. 8. The photocatalytic activities were found to be 9.1, 4.8 and 1.2 mg h^{-1} $g_{cat}{}^{-1}$ for the supported bimetallic catalysts with Ti300, Ti500 and Ti700 as the support, respectively, indicative of the highest catalytic activity of Pt(5)–Cu(1.25)/Ti300 among the catalysts. The low catalytic activity of Pt(5)–Cu(1.25)/Ti700 is understandable, which can be mainly attributed to the low BET surface area and the crystalline phase of Ti700. The low BET surface area of Ti700 (1.1 m^2 g^{-1}) results in low metal dispersion and large metal particles and thus few active sites for nitrate reduction can be rationally expected. In addition, Ti700 consists of rutile phase, which is believed to be less photocatalytically active compared to anatase phase [61]. The higher photocatalytic activity of Pt(5)–Cu(1.25)/Ti300 than that of Pt(5)–Cu(1.25)/Ti500 seems contradictory to the fact that TiO_2 with high anatase content generally shows higher photocatalytic activity compared to that with low anatase content [62,63]. It is noteworthy that the higher BET surface area of Ti300 compared to Ti500 leads to a higher Pt–Cu alloy dispersion and to smaller metal particle sizes, giving rise to more active sites for the reduction of nitrate and nitrite and to enhanced Schottky barrier effect [64]. Furthermore, the enhanced photocatalytic activity by metallization is generally more prominent for TiO_2 with lower anatase content [65,66], which eventually results in a higher catalytic activity of Pt(5)–Cu(1.25)/Ti300 compared to Pt(5)–Cu(1.25)/Ti500. For N_2 selectivity, XRD results, IR spectra of CO adsorption and XPS analysis demonstrate the similar composition of Pt–Cu alloy present in both Pt(5)–Cu(1.25)/Ti300 and Pt(5)–Cu(1.25)/Ti500 and, therefore, a similar N_2 selectivity can be expected. The slightly higher N_2 selectivity of Pt(5)–Cu(1.25)/Ti300 than Pt(5)–Cu(1.25)/Ti500 is probably attributed to the comparably high rate of nitrate reduction to nitrite, leading to a high adsorbed nitrite concentration on Pt metal surface and eventually to the facile generation of N–N bond over Pt metal surface [67,68].

Pt/Cu ratio is also an important factor controlling the photocatalytic behavior of supported bimetallic catalyst. A high content of Cu or Pt favors nitrate conversion to nitrite or nitrite to N_2/ammonia, respectively. The photocatalytic nitrate reduction over Pt(5)–Cu(0.83)/Ti300, Pt(5)–Cu(1.25)/Ti300 and Pt(5)–Cu(2.5)/Ti300 is presented in Fig. 9. The photocatalytic activities were 1.1, 9.1 and 9.8 mg h^{-1} $g_{cat}{}^{-1}$ for Pt(5)–Cu(0.83)/Ti300, Pt(5)–Cu(1.25)/Ti300 and Pt(5)–Cu(2.5)/Ti300, respectively, indicating an enhanced catalytic activity of supported bimetallic cata-

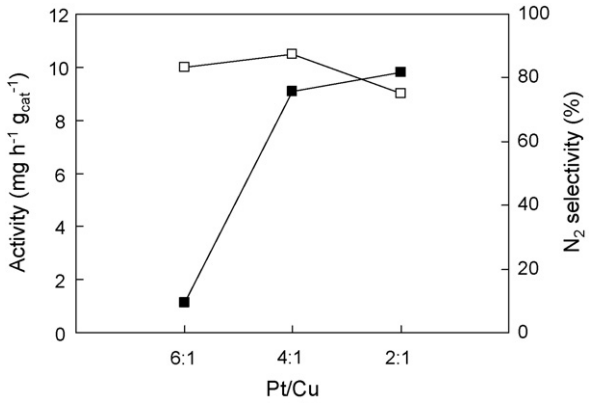

Fig. 9. Catalytic activities and N_2 selectivities of Pt(5)–Cu(0.83)/Ti300, Pt(5)–Cu(1.25)/Ti300 and Pt(5)–Cu(2.5)/Ti300. Filled symbols denote catalytic activities and open symbols denote N_2 selectivities.

lyst with increased Cu content. In contrast to Pt(5)–Cu(0.83)/Ti300 and Pt(5)–Cu(1.25)/Ti300, a substantial nitrite was found to be residual even after reaction for 4 h for the photocatalytic nitrate reduction over Pt(5)–Cu(2.5)/Ti300. IR spectra of CO adsorption indicates a low Cu content in Pt–Cu alloy in Pt(5)–Cu(0.83)/Ti300, resulting in a low rate of nitrate conversion to nitrite as well as low catalytic activity. In contrast, CO adsorption demonstrates the presence of Cu rich Pt–Cu alloy in Pt(5)–Cu(2.5)/Ti300, giving rise to a higher nitrate conversion rate. However, the high Cu content in Pt–Cu alloy correspondingly leads to fewer Pt sites, which is detrimental to further nitrite conversion to N_2/ammonia.

The catalytic behavior of the supported bimetallic catalysts is also dependent on the metal loading amount. Fig. 10 shows photocatalytic nitrate reduction over Pt(3)–Cu(0.75)/Ti300, Pt(5)–Cu(1.25)/Ti300 and Pt(7)–Cu(1.75)/Ti300. The catalytic activities were found to be 1.2, 9.1 and 4.9 mg h^{-1} $g_{cat}{}^{-1}$ for Pt(3)–Cu(0.75)/Ti300, Pt(5)–Cu(1.25)/Ti300 and Pt(7)–Cu(1.75)/Ti300, respectively. The lower nitrate conversion over Pt(3)–Cu(0.75)/Ti300 is attributed to the fewer metal sites for the reduction of nitrate and nitrite. The nitrate reduction was markedly enhanced over Pt(5)–Cu(1.25)/Ti300, while further increasing metal loading leads to a decreased catalytic activity. Although a relatively large amount of active sites for the reduction of nitrate or nitrite are available over Pt(7)–Cu(1.75)/Ti300, the high metal loading may also be detrimental to the photo-induction effect of TiO_2 support via the shield-effect [59,60]. In addition, the catalyst with higher catalytic activities shows higher N_2 selectivities. The higher N_2 selectivity can be attributed to the high nitrite coverage on metallic Pt sites due to higher nitrate conversion rate, leading to the facile generation of N_2 instead of ammonia [67,68].

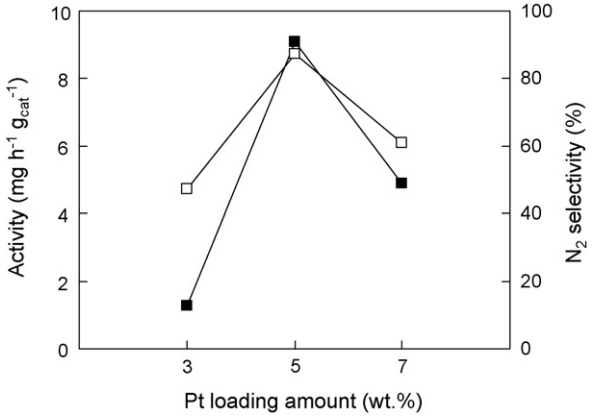

Fig. 10. Catalytic activities and N_2 selectivities of Pt(3)–Cu(0.75)/Ti300, Pt(5)–Cu(1.25)/Ti300 and Pt(7)–Cu(1.75)/Ti300. Filled symbols denote catalytic activities and open symbols denote N_2 selectivities.

4. Conclusions

In this study, TiO_2 supported Pt–Cu bimetallic catalysts were tested for the photocatalytic removal of aqueous nitrate in the presence of benzene. In contrast to the supported monometallic catalysts, TiO_2 supported Pt–Cu bimetallic catalysts are proved to be active for selective nitrate reduction. The catalytic behavior of the bimetallic catalyst for photocatalytic nitrate reduction is strongly associated with the properties of TiO_2 supports, metal loading amount and Pt/Cu ratio. High Pt–Cu alloy dispersion as well as small metal particle size can be achieved over TiO_2 calcined at low temperature, which favors the selective nitrate reduction. Increasing Cu content in the bimetallic catalysts leads to the increased Cu content in Pt–Cu alloy and enhances nitrate reduction to nitrite, while high Cu content in Pt–Cu alloy is detrimental to N_2 selectivity of the bimetallic catalysts. Higher metal loading provides more active sites for nitrate reduction, whereas the excessively high metal loading invokes the shield-effect which suppresses the catalytic activity and N_2 selectivity of the catalyst for photocatalytic nitrate reduction.

Acknowledgements

This work was supported by the National Natural Science Foundation of China (Nos. 20677026, 20637030 and 20877039), Scientific and Technical Supporting Programs of China (2006BAC02A15) and Program of New Century Excellent Talents in University (NCET).

Appendix A. Supplementary data

Supplementary data associated with this article can be found, in the online version, at doi:10.1016/j.jphotochem.2010.04.003.

References

[1] F.T. Wakida, D.N. Lerner, Non-agricultural sources of groundwater nitrate: a review and case study, Water Res. 39 (2005) 3–16.
[2] K. Pond, Y. Huang, Y. Wang, C.F. Kulpa, Hydrogen isotopic composition of individual n-alkanes as an intrinsic tracer for bioremediation and source identification of petroleum contamination, Environ. Sci. Technol. 36 (2002) 724–728.
[3] U.S. Environmental Protection Agency, Drinking Water Regulations and Health Advisories, U.S. Environmental Protection Agency, Washington, DC, 2006, p. 9.
[4] E.A. Edwards, L.E. Wills, M. Reinhard, D. Grbic-Galic, Anearobic degradation of toluene and xylene by aquifer microorganisms under sulfate-reducing conditions, Appl. Environ. Microbiol. 58 (1992) 794–800.
[5] A.A.M. Langenhoff, A.J.B. Zehnder, G. Schraa, Behaviour of toluene, benzene and naphthalene under anaerobic conditions in sediment columns, Biodegradation 7 (1996) 267–274.
[6] K.-D. Vorlop, T. Tacke, Erste Schritte auf dem Weg zur Edelmetall-katalysierten Nitrat- und Nitritentfernung aus Trinkwasser, Chem. Ing. Tech. 61 (1989) 836–837.
[7] A. Pintar, Catalytic processes for the purification of drinking water and industrial effluents, Catal. Today 77 (2003) 451–465.
[8] J.A. Cunningham, H. Rahme, G.D. Hopkins, C. Lebron, M. Reinhard, Enhanced in situ bioremediation of BTEX-contaminated groundwater by combined injection of nitrate and sulfate, Environ. Sci. Technol. 35 (2001) 1663–1670.
[9] C.S. Turchi, D.F. Ollis, Mixed reactant photocatalysis:intermediates and mutual rate inhibition, J. Catal. 119 (1989) 483–496.
[10] M.A. Fox, M.T. Dulay, Heterogeneous photocatalysis, Chem. Rev. 93 (1993) 341–357.
[11] M.R. Hoffmann, S.T. Martin, W. Choi, D.W. Bahnemann, Environmental applications of semiconductor photocatalysis, Chem. Rev. 95 (1995) 69–96.
[12] A.L. Linsebigler, G. Lu, J.T. Yates Jr., Photocatalysis on TiO_2 surfaces: principles, mechanisms, and selected results, Chem. Rev. 95 (1995) 735–758.
[13] I. Izumi, W.W. Dunn, K.O. Wllbourn, F.R.F. Fan, A.J. Bard, Heterogeneous photocatalytic oxidation of hydrocarbons on platinized TiO_2 powders, J. Phys. Chem. 84 (1980) 3207–3210.
[14] K. Hashimoto, T. Kawai, T. Sakata, Photocatalytic reactions of hydrocarbons and fossil fuels with water. Hydrogen production and oxidation, J. Phys. Chem. 88 (1984) 4083–4088.

[15] H. Kato, A. Kudo, Photocatalytic reduction of nitrate ions over tantalate photocatalysts, Phys. Chem. Chem. Phys. 4 (2002) 2833–2838.
[16] K.T. Ranjit, B. Viswanathan, Photocatalytic reduction of nitrite and nitrate ions over doped TiO_2 catalysts, J. Photochem. Photobiol. A: Chem. 107 (1997) 215–220.
[17] K.T. Ranjit, T.K. Varadarajan, B. Viswanathan, Photocatalytic reduction of nitrite and nitrate ions to ammonia on Ru/TiO_2 catalysts, J. Photochem. Photobiol. A: Chem. 89 (1995) 67–68.
[18] J. Sá, C. Alcaraz Agüera, S. Gross, J.A. Anderson, Photocatalytic nitrate reduction over metal modified TiO_2, Appl. Catal. B: Environ. 85 (2009) 192–200.
[19] B. Bems, F.C. Jentoft, R. Schlogl, Photoinduced decomposition of nitrate in drinking water in the presence of titania and humic acids, Appl. Catal. B: Environ. 20 (1999) 155–163.
[20] T. Mori, J. Suzuki, K. Fujimoto, M. Watanabe, Y. Hasegawa, Reductive decomposition of nitrate ion to nitrogen in water on a unique hollandite photocatalyst, Appl. Catal. B: Environ. 23 (1999) 283–289.
[21] H. Kominami, T. Nakaseko, Y. Shimada, A. Furusho, H. Inoue, S. Murakami, Y. Kera, B. Ohtani, Selective photocatalytic reduction of nitrate to nitrogen molecules in an aqueous suspension of metal-loaded titanium(IV) oxide particles, Chem. Commun. (2005) 2933–2935.
[22] F. Zhang, R. Jin, J. Chen, C. Shao, W. Gao, L. Li, N. Guan, High photocatalytic activity and selectivity for nitrogen in nitrate reduction on Ag/TiO_2 catalyst with fine silver clusters, J. Catal. 232 (2005) 424–431.
[23] B. Ohtani, M. Kakimoto, H. Miyadzu, S. Nishimoto, T. Kagiya, Effect of surface-adsorbed 2-propanol on the photocatalytic reduction of silver and/or nitrate ions in acidic TiO_2 suspension, J. Phys. Chem. 92 (1988) 5773–5777.
[24] H. Kominami, A. Furusho, S. Murakami, H. Inoue, Y. Kera, B. Ohtani, Effective photocatalytic reduction of nitrate to ammonia in an aqueous suspension of metal-loaded titanium(IV) oxide particles in the presence of oxalic acid, Catal. Lett. 76 (2001) 31–34.
[25] W. Gao, R. Jin, J. Chen, X. Guan, H. Zeng, F. Zhang, N. Guan, Titania-supported bimetallic catalysts for photocatalytic reduction of nitrate, Catal. Today 90 (2004) 331–336.
[26] J. Lin, Y. Lin, P. Liu, M.J. Meziani, L.F. Allard, Y.J. Sun, Hot-fluid annealing for crystalline titanium dioxide nanoparticles in stable suspension, J. Am. Chem. Soc. 124 (2002) 11514–11518.
[27] American Public Health Association, Standard Methods for the Examination of Water and Wastewater, 18th edition, American Public Health Association, Washington, DC, 1992, pp. 516–530.
[28] S.K. Samantaray, P. Mohapatra, K. Parida, Physico-chemical characterisation and photocatalytic activity of nanosized SO_4^{2-}/TiO_2 towards degradation of 4-nitrophenol, J. Mol. Catal. A: Chem. 198 (2003) 277–287.
[29] G. Colón, M.C. Hidalgo, J.A. Navio, Photocatalytic behaviour of sulphated TiO_2 for phenol degradation, Appl. Catal. B: Environ. 45 (2003) 39–50.
[30] V. Baglio, A. Stassi, A. Di Blasi, C. D'Urso, V. Antonucci, A.S. Arico, Investigation of bimetallic Pt–M/C as DMFC cathode catalysts, Electrochim. Acta 53 (2007) 1360–1364.
[31] S.M. Augustine, W.M.H. Sachtler, Catalytic probe for alloy formation in supported PtRe catalysts, J. Catal. 106 (1987) 417–427.
[32] S.M. Augustine, W.M.H. Sachtler, Variation of catalytic activity over $PtRe/\gamma$-Al_2O_3, J. Phys. Chem. 91 (1987) 5953–5956.
[33] C.D. Wagner, L.E. Davis, M.V. Zeller, J.A. Taylor, R.M. Raymond, L.H. Gale, Empirical atomic sensitivity factors for quantitative analysis by electron spectroscopy for chemical analysis, Surf. Interface Anal. 3 (1981) 211–225.
[34] G.G. Jernigan, G.A. Somorjai, Carbon monoxide oxidation over three different oxidation states of copper: metallic copper, copper (I) Oxide, and copper (II) oxide—a surface science and kinetic study, J. Catal. 147 (1994) 567–577.
[35] P. Larsson, A. Andersson, Complete oxidation of CO, ethanol, and ethyl acetate over copper oxide supported on titania and ceria modified titania, J. Catal. 179 (1998) 72–89.
[36] N.N. Hoover, B.J. Auten, B.D. Chandler, Tuning supported catalyst reactivity with dendrimer-templated Pt–Cu nanoparticles, J. Phys. Chem. B 110 (2006) 8606–8612.
[37] S. Hufner, G.K. Wertheim, Core-line asymmetries in the X-ray-photoemission spectra of metals, Phys. Rev. B 11 (1975) 678–683.
[38] S.H. Chien, M.C. Kuo, C.H. Lu, K.N. Lu, Spectroscopic studies of NO reduction on Pt/TiO_2 catalysts, Catal. Today 97 (2004) 121–127.
[39] R.P. Eischens, W.A. Pliskin, The infrared spectra of adsorbed molecules, Adv. Catal. 10 (1958) 1–56.
[40] L.L. Sheu, Z. Karpinski, W.M.H. Sachtler, Effects of palladium particle size and palladium silicide formation on Fourier transform infrared spectra of CO adsorbed on Pd/SiO_2 catalysts, J. Phys. Chem. 93 (1989) 4890–4894.
[41] X. Zhu, Y. Xie, C. Liu, Y. Zhang, Stability of Pt particles on ZrO_2 support during partial oxidation of methane: DRIFT studies of adsorbed CO, J. Mol. Catal. A: Chem. 282 (2008) 67–73.
[42] H. Song, R.M. Rioux, J.D. Hoefelmeyer, R. Komor, K. Niesz, M. Grass, P. Yang, G.A. Somorjai, Hydrothermal growth of mesoporous SBA-15 silica in the presence of PVP-stabilized Pt nanoparticles: synthesis, characterization, and catalytic properties, J. Am. Chem. Soc. 128 (2006) 3027–3037.
[43] M. Primet, J.M. Basset, M.V. Mathieu, M. Prettre, Infrared study of CO adsorbed on $Pt\,Al_2O_3$. A method for determining metal–adsorbate interactions, J. Catal. 29 (1973) 213–223.
[44] R. Barth, R. Pitchai, R.L. Anderson, X.E. Verykios, Thermal desorption-infrared study of carbon monoxide adsorption by alumina-supported platinum, J. Catal. 116 (1989) 61–70.
[45] E.S. Shpiro, O.P. Tkachenko, N.I. Jaeger, G. Schulz-Ekloff, W. Gru1nert, Structure and reactivity of platinum–copper alloy particles supported on ZSM-5, J. Phys. Chem. B 102 (1998) 3798–3805.
[46] L.L. Perissinotti, M.A. Brusa, M.A. Grela, Yield of carboxyl anion radicals in the photocatalytic degradation of formate over TiO_2 particles, Langmuir 17 (2001) 8422–8427.
[47] W.Y. Teoh, L. Mädler, R. Amal, Inter-relationship between Pt oxidation states on TiO_2 and the photocatalytic mineralisation of organic matters, J. Catal. 251 (2007) 271–280.
[48] S. Bae, K.L. Stewart, A.A. Gewirth, Nitrate adsorption and reduction on Cu(1 0 0) in acidic solution, J. Am. Chem. Soc. 129 (2007) 10171–10180.
[49] F. Epron, F. Gauthard, C. Pinéda, J. Barbier, Catalytic reduction of nitrate and nitrite on $Pt–Cu/Al_2O_3$ catalysts in aqueous solution: role of the interaction between copper and platinum in the reaction, J. Catal. 198 (2001) 309–318.
[50] J.A. Navio, G. Colon, M. Trillas, J. Peral, X. Domenech, J.J. Testa, J. Padron, D. Rodriguez, M.I. Litter, Heterogeneous photocatalytic reactions of nitrite oxidation and Cr(VI) reduction on iron-doped titania prepared by the wet impregnation method, Appl. Catal. B: Environ. 16 (1998) 187–196.
[51] A. Kudo, K. Domen, K. Maruya, T. Onishi, Reduction of nitrate ions into nitrite and ammonia over some photocatalysts, J. Catal. 135 (1992) 300–303.
[52] A. Kudo, K. Domen, K. Maruya, T. Onishi, Photocatalytic reduction of NO_3^- to form NH_3 over $Pt–TiO_2$, Chem. Lett. 16 (1987) 1019–1022.
[53] A. Patsoura, D.I. Kondarides, X.E. Verykios, Photocatalytic degradation of organic pollutants with simultaneous production of hydrogen, Catal. Today 124 (2007) 94–102.
[54] H. Reiche, W.W. Dunn, A.J. Bard, Heterogeneous photocatalytic and photosynthetic deposition of copper on TiO_2 and WO_3 powders, J. Phys. Chem. 83 (1979) 2248–2251.
[55] S. Foster, R.D. Noble, C.A. Koval, Reversible photoreductive deposition and oxidative dissolution of copper ions in titanium dioxide aqueous suspensions, Environ. Sci. Technol. 27 (1993) 350–356.
[56] S.D. Ebbesen, B.L. Mojet, L. Lefferts, In situ attenuated total reflection infrared (ATR-IR) study of the adsorption of NO_2^-, NH_2OH, and NH_4^+ on Pd/Al_2O_3 and Pt/Al_2O_3, Langmuir 24 (2008) 869–879.
[57] A. Linsebigler, C. Rusu, J.T. Yates Jr., Absence of platinum enhancement of a photoreaction on TiO_2–CO photooxidation on Pt/TiO_2(1 1 0), J. Am. Chem. Soc. 118 (1996) 5284–5289.
[58] S.C. Sze, A.B. Mark, Preparation of highly uniform Ag/TiO_2 and Au/TiO_2 supported nanoparticle catalysts by photodeposition, Langmuir 21 (2005) 5588–5595.
[59] C.A. Emilio, M.I. Litter, M. Kunst, M. Bouchard, C. Colbeau-Justin, Phenol photodegradation on platinized-TiO_2 photocatalysts related to charge-carrier dynamics, Langmuir 22 (2006) 3606–3613.
[60] A. Maldotti, A. Molinari, G. Varani, M. Lenarda, L. Storaro, F. Bigi, R. Maggi, A. Mazzacani, G. Sartori, Immobilization of $(n\text{-}Bu_4N)_4W_{10}O_{32}$ on mesoporous MCM-41 and amorphous silicas for photocatalytic oxidation of cycloalkanes with molecular oxygen, J. Catal. 209 (2002) 210–216.
[61] T. Ohno, K. Sarukawa, M. Matsumura, Photocatalytic activities of pure rutile particles isolated from TiO_2 powder by dissolving the anatase component in HF solution, J. Phys. Chem. B 105 (2001) 2417–2420.
[62] A. Sclafani, L. Palmisano, M. Schiavello, Influence of the preparation methods of titanium dioxide on the photocatalytic degradation of phenol in aqueous dispersion, J. Phys. Chem. 94 (1990) 829–832.
[63] S. Zheng, Q. Huang, J. Zhou, B. Wang, A study on dye photoremoval in TiO_2 suspension solution, J. Photochem. Photobiol. A: Chem. 108 (1997) 235–238.
[64] M.C. Hidalgo, M. Maicu, J.A. Navıio, G. Colon, Study of the synergic effect of sulphate pre-treatment and platinisation on the highly improved photocatalytic activity of TiO_2, Appl. Catal. B: Environ. 81 (2008) 49–55.
[65] K. Tanaka, V. Capule, T. Hisanaga, Effect of crystallinity of TiO_2 on its photocatalytic action, Chem. Phys. Lett. 187 (1991) 73–76.
[66] S.K. Lee, A. Mills, Platinum and palladium in semiconductor photocatalytic systems, Platinum Metals Rev. 47 (2003) 61–72.
[67] U. Prüsse, K.-D. Vorlop, Supported bimetallic palladium catalysts for water-phase nitrate reduction, J. Mol. Catal. A: Chem. 173 (2001) 313–328.
[68] F. Deganello, L.F. Liotta, A. Macaluso, A.M. Venezia, G. Deganello, Catalytic reduction of nitrates and nitrites in water solution on pumice-supported Pd–Cu catalysts, Appl. Catal. B: Environ. 24 (2000) 265–273.